Supporting Information

Microwave-Assisted Solvothermal Synthesis of UiO-66-NH_2 and Its Catalytic Performance towards the Hydrolysis of a Nerve Agent Simulant

Zenghui Zhang, Cheng-an Tao *, Jie Zhao, Fang Wang, Jian Huang and Jianfang Wang *

College of Liberal Arts and Science, National University of Defense Technology, Changsha 410073; China; zhangch@nudt.edu.cn (Z.Z.); zhaojie15@nudt.edu.cn (J.Z.); Wangf@ nudt.edu.cn (F.W.); huangjian2015@ nudt.edu.cn (J.H.)

* Correspondence: taochengan@nudt.edu.cn(C.T.); wangjianfang@nudt.edu.cn(J.W.)

1. Size distribution of obtained MOFs

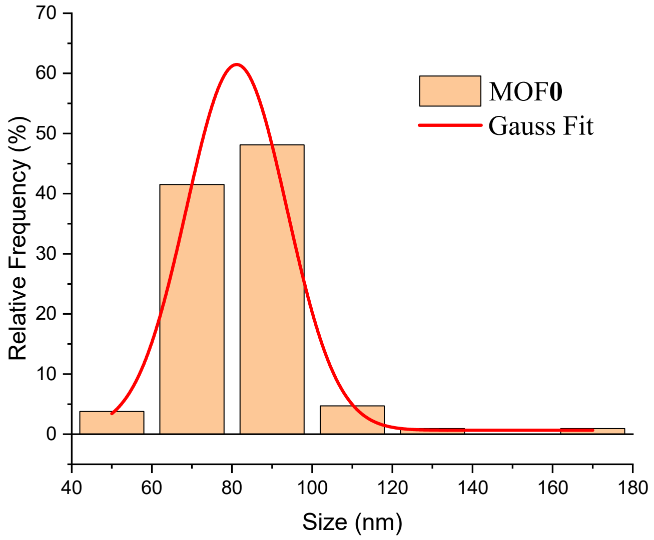

Figure S1. Size distribution of obtained MOF**0** nanocrysals

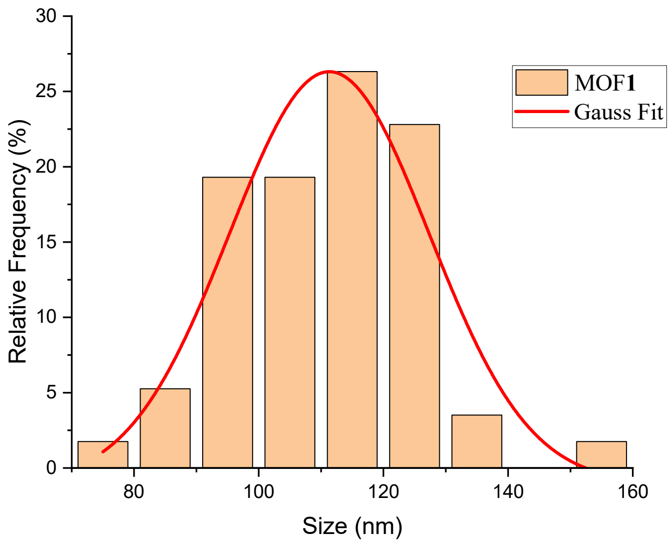

Figure S2. Size distribution of obtained MOF**1** nanocrysals

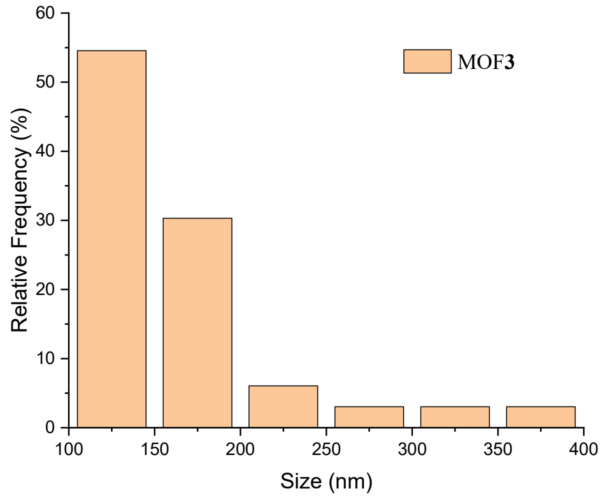

Figure S3. Size distribution of obtained MOF**3** nanocrysals

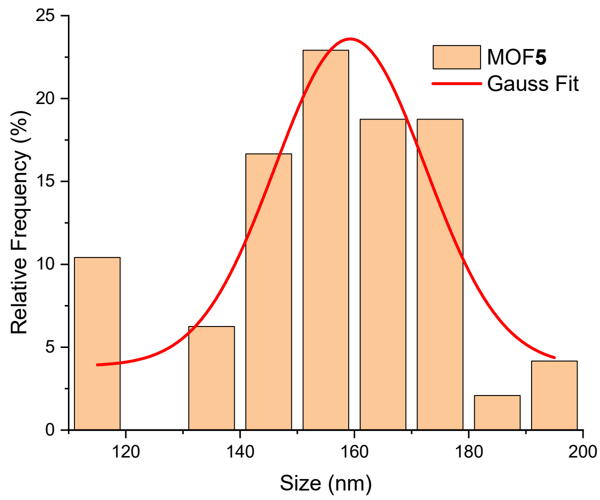

Figure S4. Size distribution of obtained MOF**5** nanocrysals

2. The pore size distribution of obtained MOFs

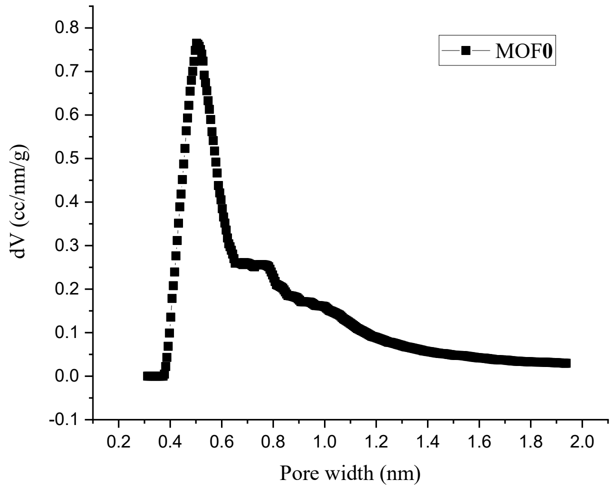

Figure S5. The micropore size of obtained MOF**0** analyzed by the Horvath–Kawazoe (HK) method

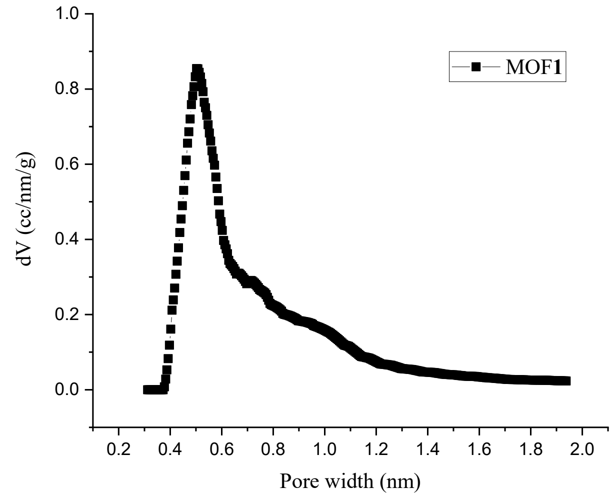

Figure S6. The micropore size of obtained MOF**1** analyzed by the HK method

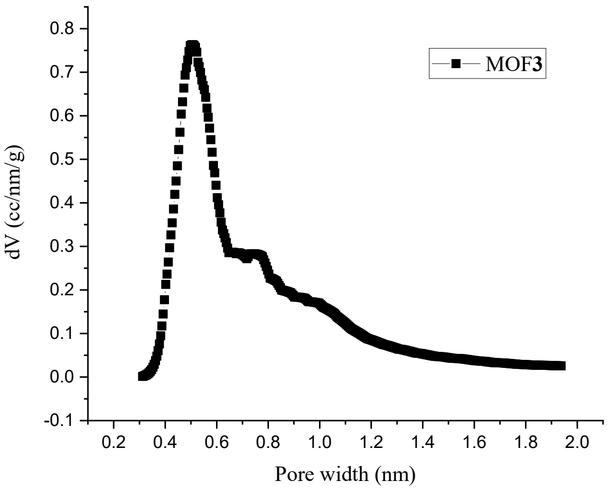

Figure S7. The micropore size of obtained MOF**3** analyzed by the HK method

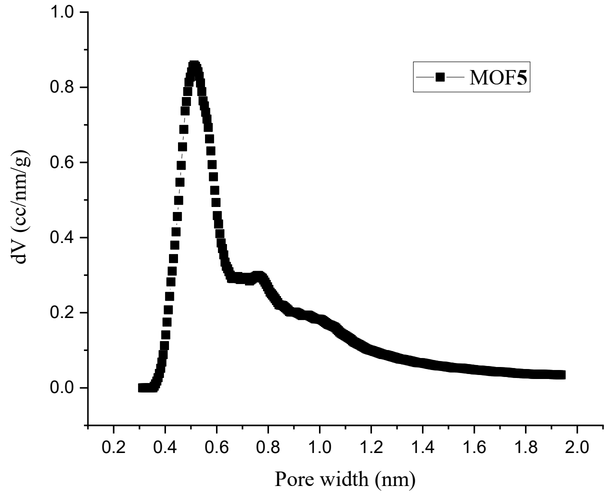

Figure S8. The micropore size of obtained MOF**5** analyzed by the HK method

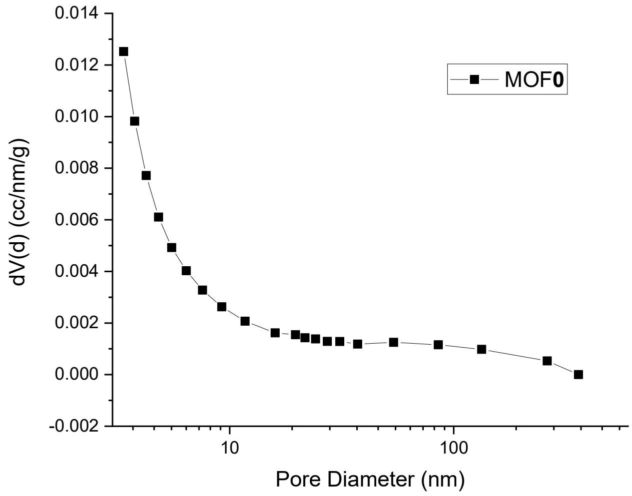

Figure S9. The Barrett-Joyner-Halenda (BJH) pore size of obtained MOF**0**

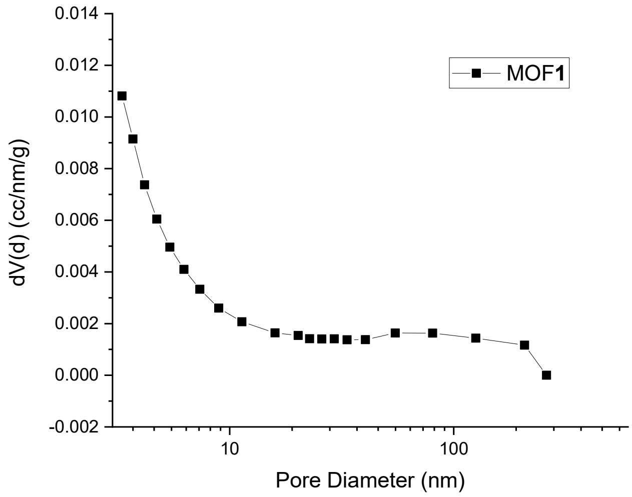

Figure S10. The BJH pore size of obtained MOF**1**

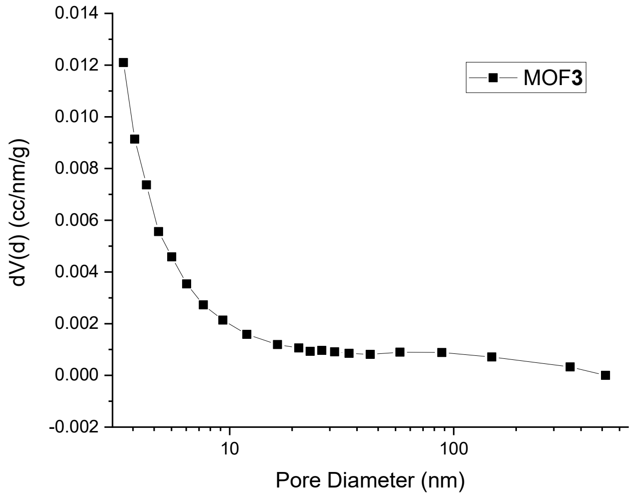

Figure S11. The BJH pore size of obtained MOF**3**

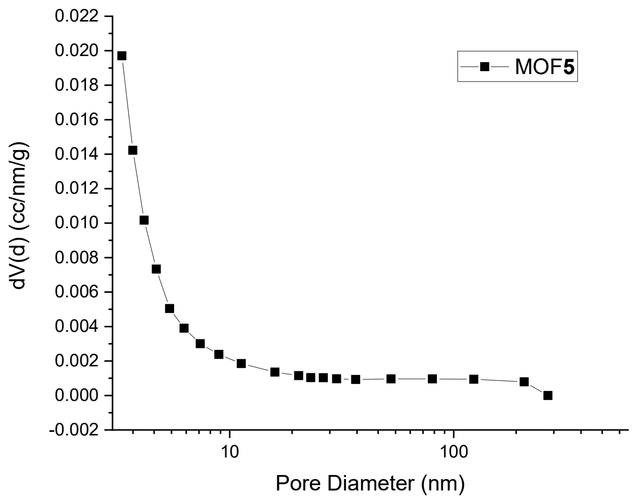

Figure S12. The BJH pore size of obtained MOF**5**

3. The NMR spectra of obtained MOFs

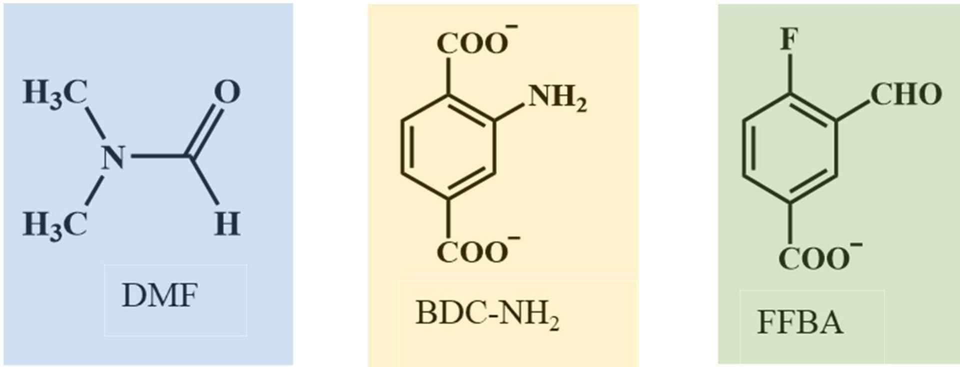

Figure S13. The chemical structures of DMF, BDC-NH_2 and FFBA in NMR test

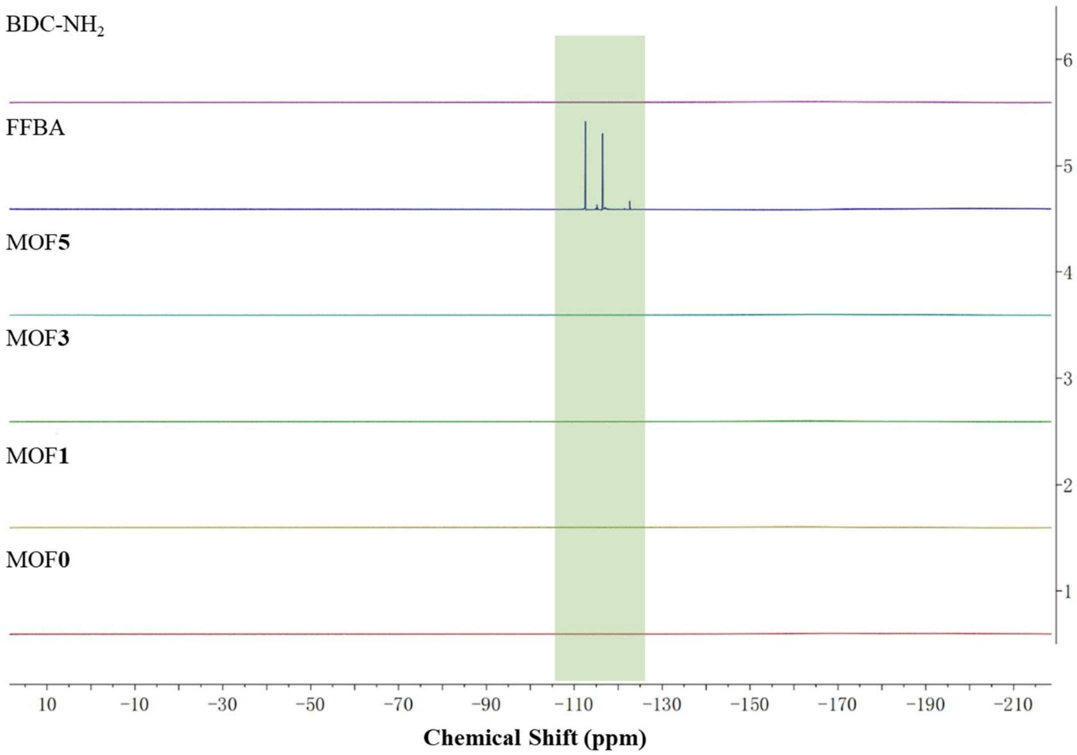

Figure S14. The ^{19}F NMR spectra of BDC-NH_2, FFBA and four obtained MOF products digested in 10wt% NaOD/D_2O

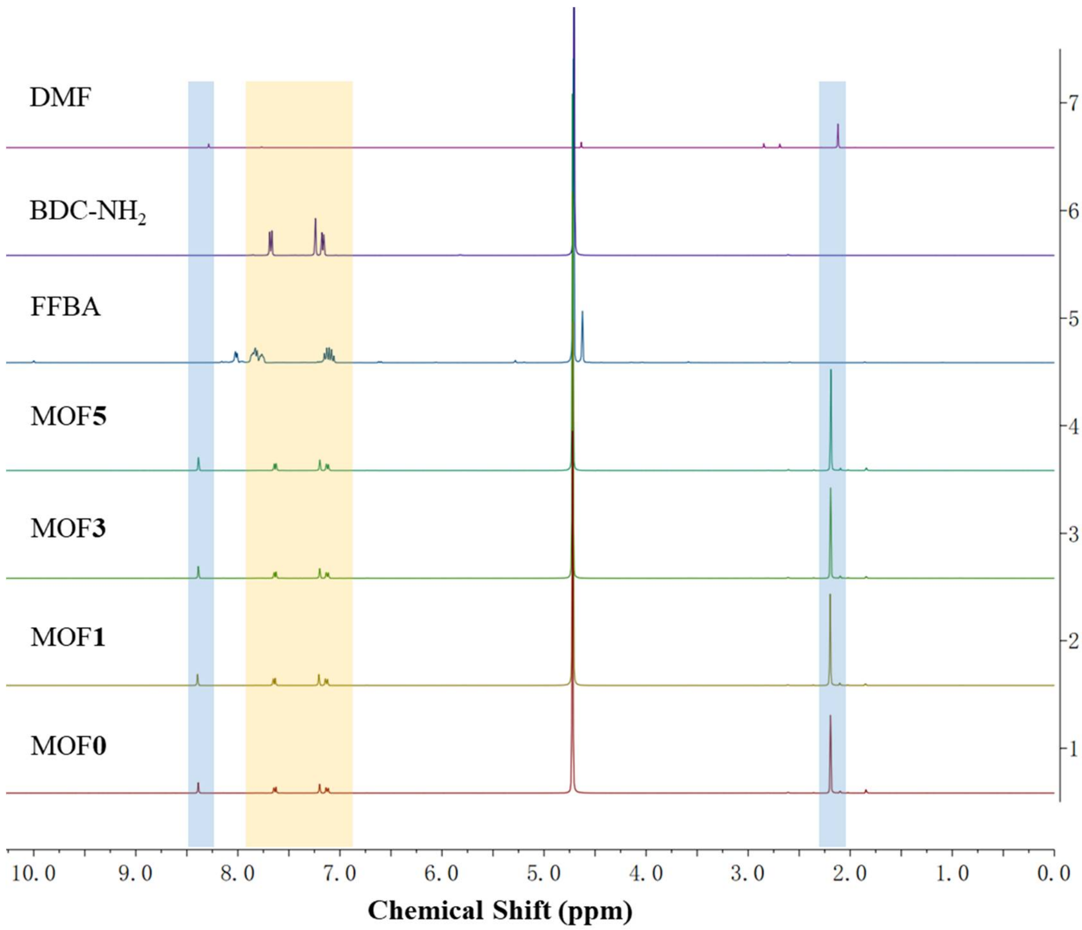

Figure S15. The ^1H NMR spectra of DMF, BDC-NH_2, FFBA and four obtained MOF products digested in 10wt% NaOD/D_2O

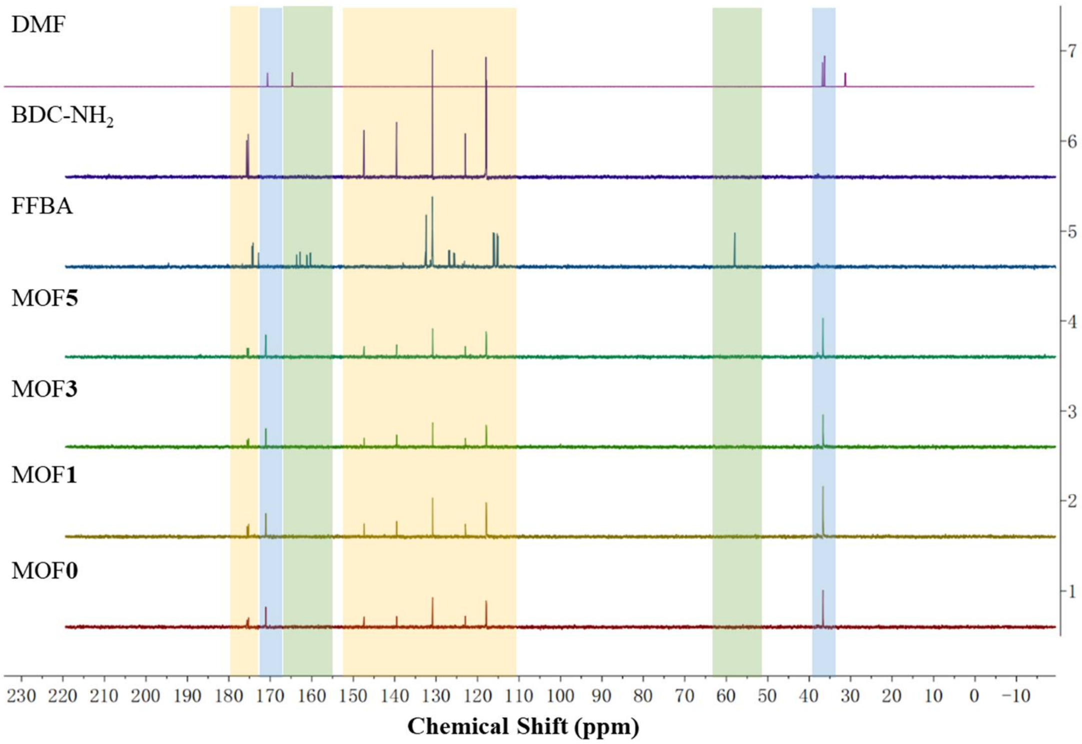

Figure S16. The ^{13}C NMR spectra of DMF, BDC-NH_2, FFBA and four obtained MOF products digested in 10wt% NaOD/D_2O

4. Observed UV-vis spectra

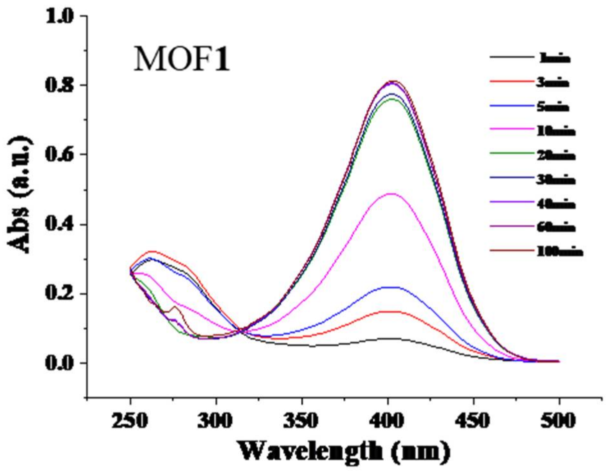

Figure S17. Hydrolysis reaction for DMNP using MOF**1** as a catalyst

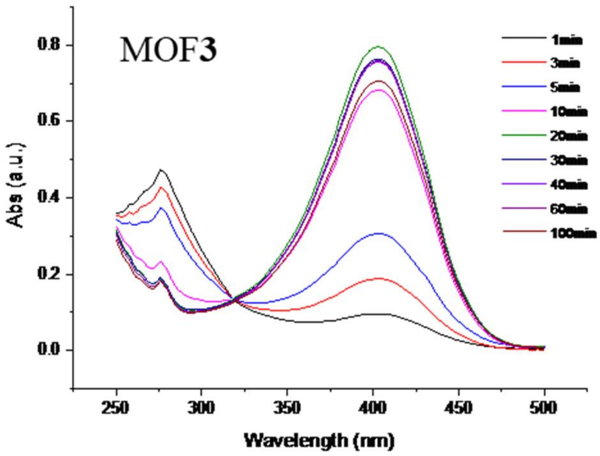

Figure S18. Hydrolysis reaction for DMNP using MOF**3** as a catalyst

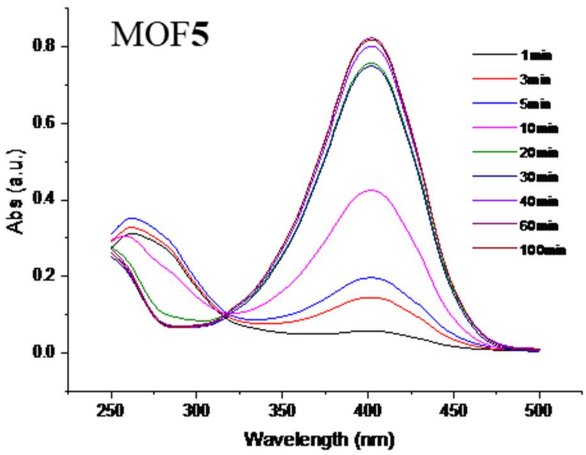

Figure S19. Hydrolysis reaction for DMNP using MOF**5** as a catalyst

5. Kinetic analysis

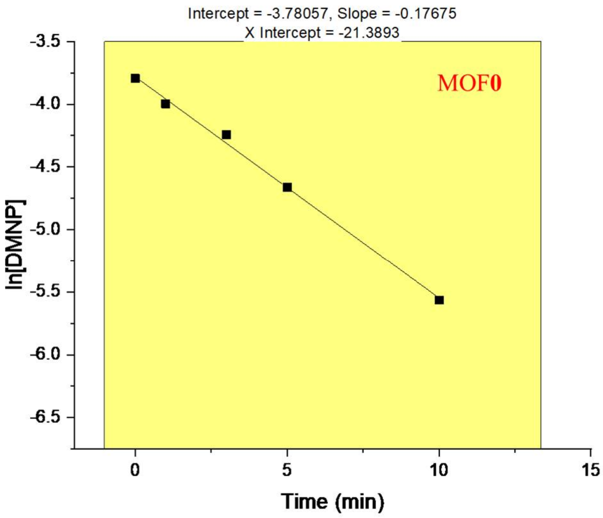

Figure S20. Kinetic analysis using MOF**0** as a catalyst.

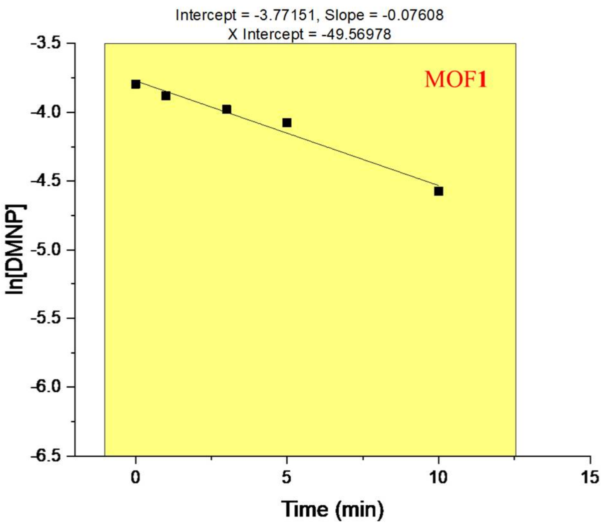

Figure S21. Kinetic analysis using MOF**1** as a catalyst.

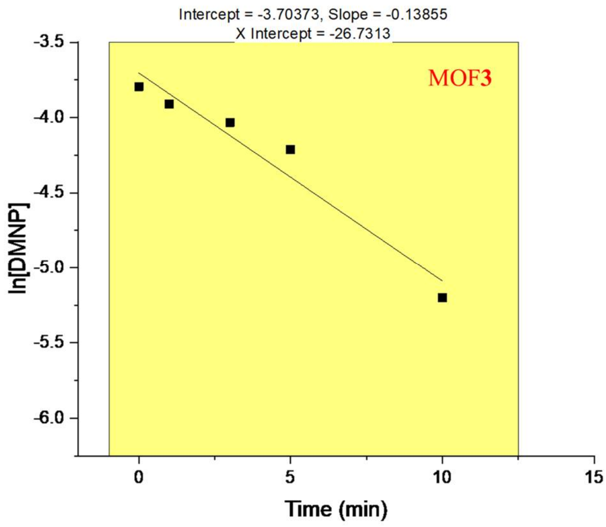

Figure S22. Kinetic analysis using MOF**3** as a catalyst.

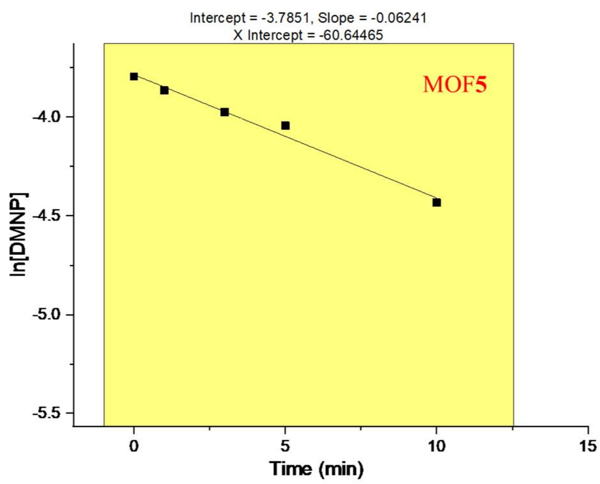

Figure S23. Kinetic analysis using MOF**5** as a catalyst.

6. The comparison of catalytic activity of Zr-MOFs reported in the literatures

Table S1. The kinetic parameters of DMNP hydrolysis catalyzed different Zr-MOFs reported in the literatures

Samples	k_1 (min^{-1})	$t_{1/2}$ (min)	Refs.
MOF**0**	0.18	3.9	This work
MOF**1**	0.08	9.1	This work
MOF**3**	0.14	5.0	This work
MOF**5**	0.06	11.1	This work
UiO-66-NH_2	0.14	4.8	[1]
UiO-66-NH_2		< 1	[2]
UiO-66-NH_2	$0.3\sim1.4\times10^{-3}$	24~495	[3]
UiO-66-NH_2	0.16	4.4	[4]
UiO-66	0.02	35	[5]
UiO-67	0.2	3.5	[6]
NU-1000	0.05	15	[7]
NU-1000(dehydrated)	0.46	1.5	[7]
MOF-808	1.40	0.5	[8]

7. References

1. Chen, R.; Tao, C.-a.; Zhang, Z.; Chen, X.; Liu, Z.; Wang, J. Layer-by-layer Fabrication of Core-Shell Fe3O4@UiO-66-NH2 with High Catalytic Reactivity toward the Hydrolysis of Chemical Warfare Agent Simulants. *ACS Applied Materials & Interfaces* **2019**, *11*, 43156–43165, doi:10.1021/acsami.9b14099.
2. Peterson, G.W.; Moon, S.; Wagner, G.W.; Hall, M.G.; Decoste, J.B.; Hupp, J.T.; Farha, O.K. Tailoring the Pore Size and Functionality of UiO-Type Metal–Organic Frameworks for Optimal Nerve Agent Destruction. *Inorganic Chemistry* **2015**, *54*, 9684–9686, doi:10.1021/acs.inorgchem.5b01867.
3. Peterson, G.W.; Destefano, M.R.; Garibay, S.J.; Ploskonka, A.M.; Mcentee, M.; Hall, M.G.; Karwacki, C.J.; Hupp, J.T.; Farha, O.K. Optimizing Toxic Chemical Removal through Defect-Induced UiO-66-NH2 Metal–Organic Framework. *Chemistry - A European Journal* **2017**, *23*, 15913–15916, doi:10.1002/chem.201704525.
4. Lu, A.X.; McEntee, M.; Browe, M.A.; Hall, M.G.; DeCoste, J.B.; Peterson, G.W. MOFabric: Electrospun Nanofiber Mats from PVDF/UiO-66-NH2 for Chemical Protection and Decontamination. *Acs Applied Materials & Interfaces* **2017**, *9*, 13632–13636, doi:10.1021/acsami.7b01621.
5. Katz, M.J.; Mondloch, J.E.; Totten, R.K.; Park, J.K.; Nguyen, S.T.; Farha, O.K.; Hupp, J.T. Simple and compelling biomimetic metal-organic framework catalyst for the degradation of nerve agent simulants. *Angewandte Chemie International Edition* **2014**, *53*, 497–501, doi:10.1002/anie.201307520.
6. Katz, M.J.; Moon, S.; Mondloch, J.E.; Beyzavi, M.H.; Stephenson, C.J.; Hupp, J.T.; Farha, O.K. Exploiting parameter space in MOFs: a 20-fold enhancement of phosphate-ester hydrolysis with UiO-66-NH2. *Chemical Science* **2015**, *6*, 2286–2291, doi:10.1039/C4SC03613A.
7. Mondloch, J.E.; Katz, M.J.; Isley, W.C.; Ghosh, P.; Liao, P.; Bury, W.; Wagner, G.W.; Hall, M.G.; Decoste, J.B.; Peterson, G.W. Destruction of chemical warfare agents using metal–organic frameworks. *Nature Materials* **2015**, *14*, 512–516, doi:10.1038/nmat4238.
8. Moon, S.-Y.; Liu, Y.; Hupp, J.T.; Farha, O.K. Instantaneous Hydrolysis of Nerve-Agent Simulants with a Six-Connected Zirconium-Based Metal–Organic Framework. *Angewandte Chemie International Edition* **2015**, *54*, 6795–6799, doi:10.1002/anie.201502155.